BBA - Bioenergetics 1860 (2019) 573–581

Contents lists available at ScienceDirect

BBA - Bioenergetics

journal homepage: www.elsevier.com/locate/bbabio

Mutations in a conserved loop in the PSST subunit of respiratory complex I affect ubiquinone binding and dynamics

Etienne Galemou Yoga[a,b,1], Outi Haapanen[c,1], Ilka Wittig[d,e], Karin Siegmund[a,b], Vivek Sharma[c,f,*], Volker Zickermann[a,b,e,**]

[a] Structural Bioenergetics Group, Institute of Biochemistry II, Medical School, Goethe-University, Frankfurt am Main, Germany
[b] Centre for Biomolecular Magnetic Resonance, Institute for Biophysical Chemistry, University of Frankfurt, Frankfurt am Main, Germany
[c] Department of Physics, University of Helsinki, Helsinki, Finland
[d] Functional Proteomics, ZBC, Medical School, Goethe University, Frankfurt am Main, Germany
[e] Cluster of Excellence Frankfurt "Macromolecular Complexes", Goethe-University, Frankfurt am Main, Germany
[f] Institute of Biotechnology, University of Helsinki, Helsinki, Finland

ARTICLE INFO

Keywords:
Cell respiration
Proton pumping
Electron transfer
Redox-coupled proton pumping
Quinone dynamics

ABSTRACT

Respiratory complex I catalyses the reduction of ubiquinone (Q) from NADH coupled to proton pumping across the inner membrane of mitochondria. The electrical charging of the inner mitochondrial membrane drives the synthesis of ATP, which is used to power biochemical reactions of the cell. The recent surge in structural data on complex I from bacteria and mitochondria have contributed to significant understanding of its molecular architecture. However, despite these accomplishments, the role of various subdomains in redox-coupled proton pumping remains entirely unclear. In this work, we have mutated conserved residues in the loop of the PSST subunit that faces the ~30 Å long unique Q-binding tunnel of respiratory complex I. The data show a drastic decrease in Q reductase activity upon mutating several residues despite full assembly of the complex. *In-silico* modeling and multiple microsecond long molecular dynamics simulations of wild-type and enzyme variants with exchanges of conserved arginine residues revealed remarkable ejection of the bound Q from the site near terminal electron donor N2. Based on experiments and long-time scale molecular simulations, we identify microscopic elements that dynamically control the diffusion of Q and are central to redox-coupled proton pumping in respiratory complex I.

1. Introduction

With more than 40 subunits and a mass of almost 1 MDa NADH:ubiquinone oxidoreductase (complex I) is the largest and most complicated enzyme of the respiratory chain [1–3]. Redox-linked proton translocation by complex I generates a substantial fraction of the proton motive force (ca. 40%) that drives ATP synthase. Complex I dysfunction is associated with a number of neuromuscular and neurodegenerative diseases [4]. Formation of reactive oxygen species (ROS) by complex I during ischemia/reperfusion plays a major role for inflicting tissue damage in myocardial infarction [5]. ROS generation is thought to be mitigated by the reversible conversion of the active (A) form into the deactive (D) form of the enzyme [6]. In the last five years several X-ray and cryoEM structures of complex I were solved [7–15]. The overall architecture of bacterial and mitochondrial complex I is now understood and comprises an L-shaped arrangement of a peripheral arm and a matrix arm (Fig. 1A). At the interface of the two arms, the reduction site for ubiquinone and its extended access pathway from the membrane [16,17] are formed by the hydrophilic PSST and 49-kDa subunits and the hydrophobic ND1 subunit (Fig. 1, see also Fig. S1). There is a wide consensus that it is the reduction of ubiquinone that triggers and drives the proton pumps [1–3], but how this is achieved at a molecular scale, remains enigmatic. We have suggested that the concerted structural rearrangement of the β1-β2 loop of the 49-kDa subunit, and the loops connecting transmembrane helices (TMH) 5 and 6 of ND1 and TMH 1 and 2 of ND3 play a key role in coupling ubiquinone (Q) reduction with proton translocation by membrane intrinsic pump elements, located as far as 200 Å from the redox active site [8].

* Correspondence to: V. Sharma, Department of Physics, University of Helsinki, Gustaf Hällströmin katu 2, 00560 Helsinki, Finland.
** Correspondence to: V. Zickermann, Goethe-University Frankfurt, Medical School, Institute of Biochemistry II, Structural Bioenergetics Group, Max-von-Laue Str. 9, 60438 Frankfurt, Germany.
E-mail addresses: vivek.sharma@helsinki.fi (V. Sharma), Zickermann@med.uni-frankfurt.de (V. Zickermann).
[1] Contributed equally.

https://doi.org/10.1016/j.bbabio.2019.06.006
Received 13 December 2018; Received in revised form 10 May 2019; Accepted 15 June 2019
Available online 19 June 2019

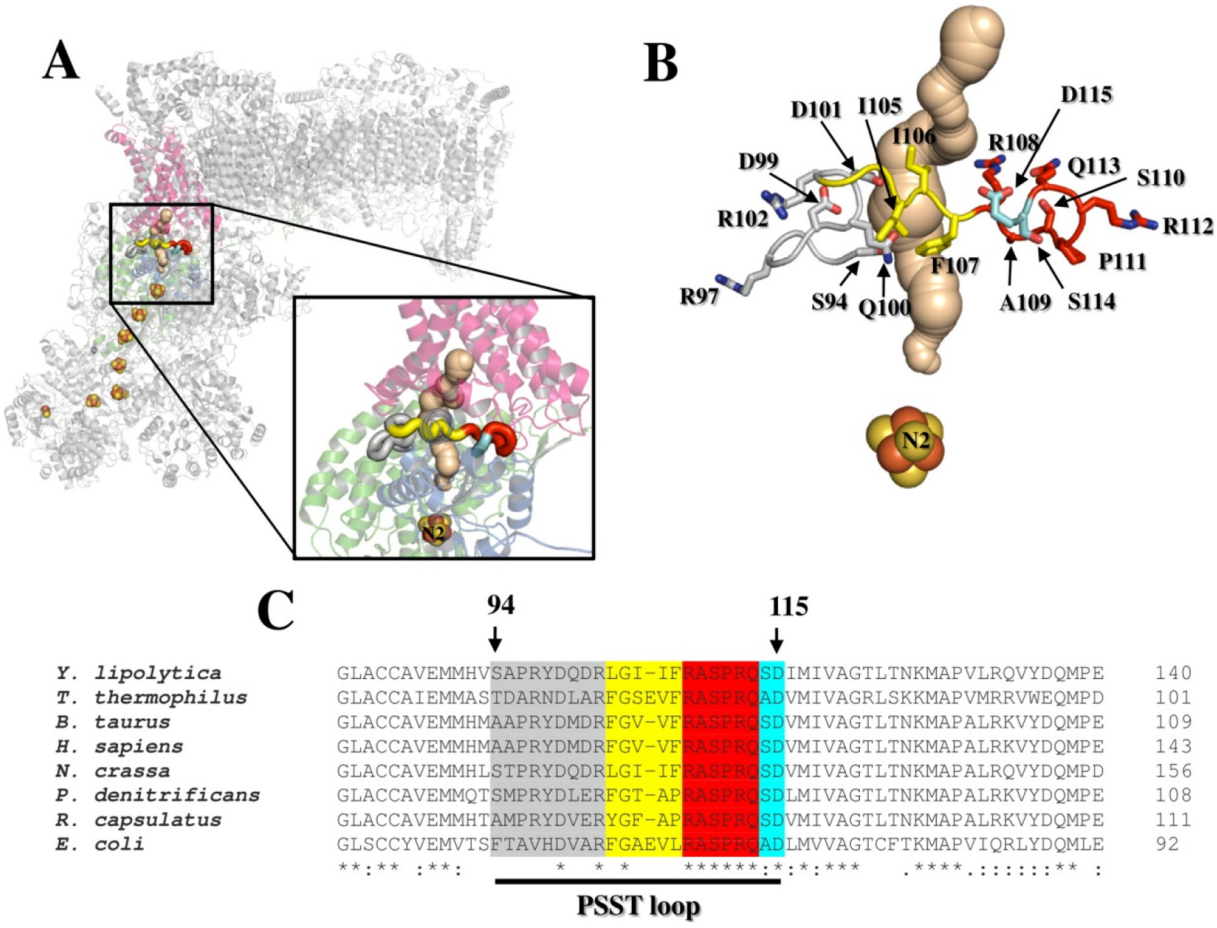

Fig. 1. A loop of subunit PSST forms an integral part of the interface of peripheral arm and membrane arm of complex I and lines the access pathway of ubiquinone. (A) Overall structure of *Yarrowia lipolytica* complex I (PDB: 6GCS; ND1, pink; 49-kDa, green; PSST, marine; all other subunits, grey). The ubiquinone binding site and access pathway (beige) was calculated with CAVER 3.0 [59] using a probe radius of 1.4 Å (starting from the hydroxyl of Y144 from 49 kDa subunit). The inset shows a magnification of the interface region with the PSST loop highlighted in color (N-terminal region, grey; hydrophobic stretch, yellow; RASPRQ motif, red; C-terminal end, cyan; β strand 1 removed for clarity). (B) The PSST loop from *Y. lipolytica* complex I (PDB: 6GCS, colored as in (A)) with selected side chains shown in stick representation. (C) Sequence alignment of PSST subunits from different organisms with colors as in panel A and B. (For interpretation of the references to color in this figure legend, the reader is referred to the web version of this article.)

Indeed, multiscale simulation approaches demonstrated redox-linked conformational changes of the ubiquinone reduction site [18,19] and suggested that ubiquinone moves in a redox-state dependent manner between distinct binding sites that are formed by conserved residue clusters [20]. The site of ubiquinone binding observed in a recent cryo-EM study [15] supported a two state stabilization change mechanism [21] for complex I and locking movement of the ND3 loop by a disulfide bond introduced by site-directed mutagenesis was shown to disengage the proton pump [22]. However, despite these significant advancements, even the basic principles of proton pumping remain unclear and are debated.

Earlier, valuable information on the function of individual residues in the Q reduction site and in the Q access path was deduced from structure guided site directed mutagenesis experiments in complex I from the aerobic yeast *Yarrowia lipolytica* [17,23]. However, a complete atomic model of the ubiquinone binding channel and the highly conserved loop in the PSST subunit became available only recently [9–15], due to the spectacular developments in cryo-EM technology. This loop forms a sector of the functionally important interface of membrane and peripheral arms and lines the extended Q binding site. Interestingly, the central segment of the loop was discussed to be related to an active site loop in CO dehydrogenase and harbors a conserved arginine residue that carries a rare posttranslational hydroxyl modification in mammalian complex I [24,25]. Taking advantage of our yeast genetic model system for eukaryotic complex I we introduced a set of point mutations in the PSST loop and studied the impact on complex I function by biochemical and molecular dynamics (MD) simulation methods. The combined data reveal coupling of the conformational dynamics of key amino acid residues in the Q-tunnel with the binding and dynamics of Q.

2. Methods

2.1. Deletion strains and site directed mutagenesis of subunit PSST from Yarrowia lipolytica

The *Yarrowia lipolytica* nukmΔ deletion strain used in this study was described previously [26]. All point mutations were generated in *E. coli* by PCR mutagenesis and then used for transformation of *Y. lipolytica* strain nukmΔ employing the one step transformation method as described [27]. After transformation into nukmΔ, plasmids were recovered, and the entire open reading frames were re-sequenced to verify the introduced mutations and to exclude others changes in the sequence.

2.2. Preparation of mitochondrial membranes and purification of complex I

Preparation of mitochondrial membranes and purification of

complex I was essentially carried out as described previously [28].

2.3. Activity measurements and proton translocation

Complex I content was assessed by following NADH oxidation in the presence of the artificial electron acceptor hexaammineruthenium (III) (HAR) [29]. This activity involves only the electron input module of complex I. The physiological electron transfer activity of complex I is typically measured using short chain ubiquinone analogues to avoid solubility problems. Here we used decylbenzoquinone (DBQ) with a linear side chain as described previously [28]. To monitor the influence of the full length isoprenoid side chain we measured electron transfer from NADH to oxygen employing native Q9 in the mitochondrial membranes. For each mutant two biological replicates were analyzed and each measurement was carried out in duplicate. Kinetic parameters for DBQ were determined for mutants with sufficient residual activity. For selected mutants we also tested ubiquinone with one (Q1) or two (Q2) isoprenoid units.

Purified complex I (200 μg) from either GB20 (parental strain) or mutant strains R108A (PSST) or R108E (PSST) was reconstituted into proteoliposomes at a protein-to-lipid ratio of 1:50 (w/w) and proton pumping was monitored by ACMA fluorescence quenching following the protocol described earlier [30]. Fluorescence changes were monitored at 30 °C in a Flurolog-3 spectrofluorometer (Horiba scientific). 0.5 μM ACMA, 60 μM DBQ, 100 μM NADH and 1 μM DQA or 1 μM FCCP were added after 20 s, 50 s 100 s, 320 s respectively.

2.4. Electrophoresis

Mitochondrial membranes from *Y. lipolytica* were solubilized in 1.0 g/g DDM, respectively and separated by blue native electrophoresis (BN-PAGE) with a 4–16% acrylamide gradient [31]. Complex I in gel activity was performed as described previously [32].

2.5. Mass spectrometry

1 μl complex I (75 μg) was resuspended in 75 μl 6 M guanidiniumhydrochlorid (GdmCl), 50 mM Tris/HCl, pH 8.5, 10 mM Tris(2-carboxyethyl)phosphine (TCEP) and incubated at 95 °C for 5 min. Reduced thiols were alkylated with 40 mM chloroacetamid. Samples were diluted with 25 mM Tris/HCl, pH 7.5, 10% acetonitrile to obtain a final GdmCl concentration of 0.6 M. Samples were divided into 3 parts. Proteins were digested with Trypsin, or LysC + GluC (0.1 μg protease/25 μg protein, sequencing grade, Promega) overnight at 37 °C under gentle agitation. Digestion was stopped by adding trifluoroacetic acid to a final concentration of 0.5%. Peptides were purified on multi-stop-and-go tip (StageTip) containing three C18 discs [33]. Liquid chromatography/mass spectrometry (LC/MS) was performed on Thermo Scientific™ Q Exactive Plus equipped with an ultra-high performance liquid chromatography unit (Thermo Scientific Dionex Ultimate 3000) and a Nanospray Flex Ion-Source (Thermo Scientific).

MS Data were analyzed by Peaks7 Proteomics software (Bioinformatics solution).

2.6. Computational methods

We performed fully atomistic classical molecular dynamics (MD) simulations on complex I structures from *Thermus thermophilus* (*T.t.*), *Yarrowia lipolytica* (*Y.l.*) and *Bos taurus* (*B.t.*) (PDB id 4HEA [7], 6GCS [15] and 5LC5 [9], respectively). Our model systems (~230,000 atoms) comprised subunits ND1, ND3, 49 kDa, PSST, 30 kDa, TYKY and one subunit specific to *Thermus* enzyme in full lipid-solvent environment. The smaller model systems allowed for remarkably long simulation times and multiple simulation replicas, which are necessary to decipher the movement of Q molecule in the ~30 Å long Q tunnel.

Some of the missing parts in protein structures were modeled. For instance, the missing loop in the PSST subunit in the *Thermus* structure was modeled with the MODELLER program [34]. Similarly, the missing amino acid side chains in bovine and *Yarrowia* enzymes were also modeled and energy minimized. The N terminus (amino acids 1 to 43) of core subunit 49 kDa in *B.t.* complex I was removed to keep the model system size computationally tractable. Similarly, highly flexible N and C terminals (50–79 in 49 kD, 42–52 in PSST, 116 to 124 in ND3 and 50 to 65 in TYKY) were removed in *Y.l.* complex I. We obtained the initial protein-membrane models from CHARMM-GUI [35–37] using OPM aligned structures [38]. Since no complex I structures with quinone in the Q binding cavity is available, we modeled and relaxed the quinone as before [19,39]. In the case of *Y.l.* setup, we used the coordinates of Q head group provided in [15] to model the Q in the Q-tunnel. Subsequently, we added TIP3 water molecules and neutralized and ionized the system with NaCl (100 mM), after which the system was minimized with weak constraints (2000 kJ mol^{-1} nm^{-2}) applied on the protein. Keeping the constraints, the system was equilibrated in NVT conditions for 100 ps and in NPT conditions for 1 ns. Next, we removed the constraints and energy minimized the entire system, followed by 100 ps NVT and 10 ns NPT equilibration MD runs. In production MD, we used Nosé-Hoover thermostat [40,41] and Parrinello-Rahman barostat [42,43] as implemented in Gromacs [44]. The temperature and pressure were kept to 310 K temperature and 1 atm, respectively. We used Gromacs 5.1.4 [44] with CHARMM22/36 [45–47] force field with derived parameters for lipids, ions, protein, water, quinone [48] and FeS clusters [49].

We analyzed in detail the dynamic behavior of the R112 (PSST)-E218 (ND1) ion pair and its effect on Q dynamics in wild-type and mutant cases. We performed multiple simulations on the R112A mutant, and also on the R108E variant, which represents a charge change of $-2e$, and which is expected to reveal distinct effects in classical MD simulations.

To further explore the coupled dynamics of Arg-Glu ion-pair and Q, and to enhance the diffusion of the Q molecule in the cavity, we performed three ~350 ns MD runs on *B.t.* system by restraining the distance between the two residues (R112 and E218) to ca. 15 Å with a harmonic force constant of ca. 2000 kJ mol^{-1} nm^{-2}. Three independent runs were made, and in all we observed rapid (after ca. 200 ns) diffusion of Q molecule. All model systems and their simulation times are displayed in Table S4.

3. Results

The long loop following helix α2 of subunit PSST consists of 22 residues ranging from S94 to D115 in complex I from *Y. lipolytica* (Fig. 1). It forms a substantial part of the interface of membrane arm and peripheral arm and its central segment lines the access pathway for substrate to the Q reduction site (Fig. 1A, B). A sequence alignment of PSST orthologues from different species showed that the loop comprises several highly conserved arginine and polar residues (Fig. 1C) including a C-terminal RXSPRQ motif with X being either an alanine residue or a proline. This motif is preceded by a short and less well conserved hydrophobic stretch that typically harbors a phenylalanine residue. We generated 27 point mutations in 14 positions in the PSST interface loop of complex I from *Y. lipolytica* and analyzed their effect on complex I assembly and function. Except for A109F, mitochondrial membranes from all mutants analyzed in this study showed a complex I content comparable with the parental strain as determined by assessing the NADH:hexaammineruthenium (NADH:HAR) electron transfer activity and by BN-PAGE (Table S1, Fig. S2), indicating that assembly and stability of the complex was not disturbed by exchanges in the loop.

3.1. Mutations in the N-terminal loop region and the intersecting hydrophobic stretch

The N-terminal segment of the PSST loop harbors a number of

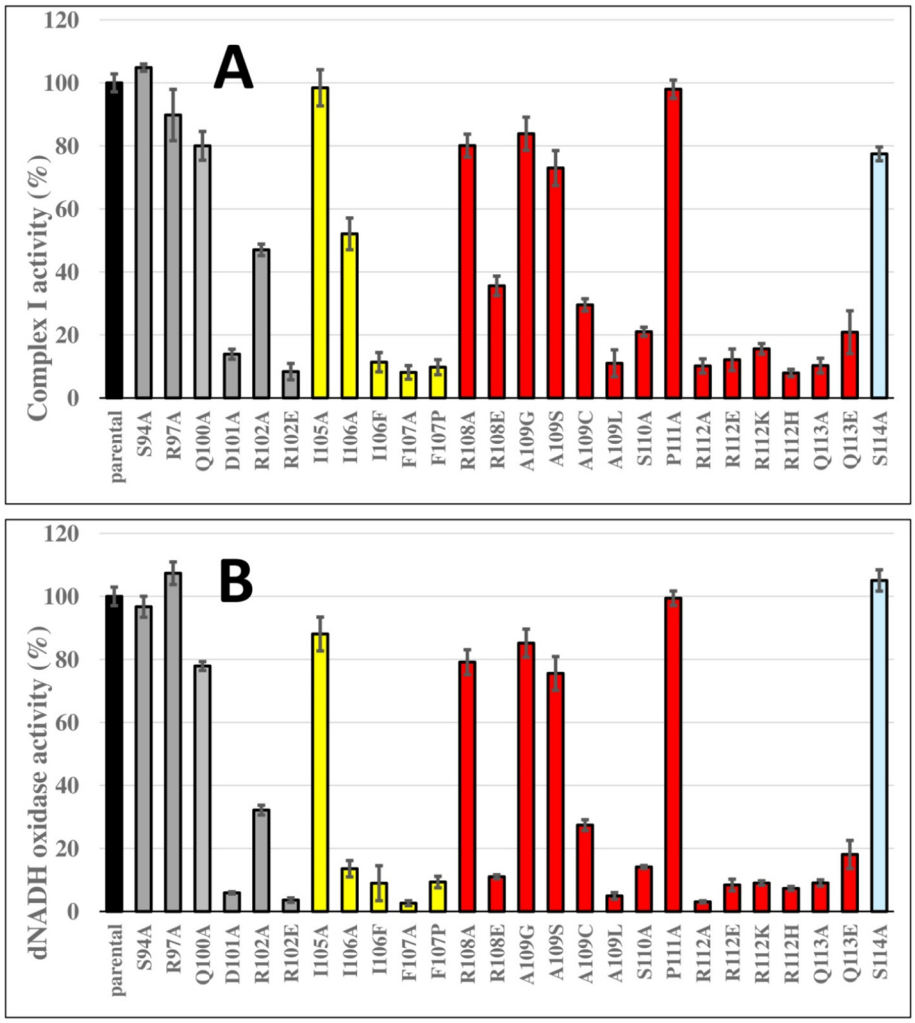

Fig. 2. Ubiquinone reductase and NADH oxidase activities of mitochondrial membranes from parental strain and site directed mutants.
(A) Relative inhibitor sensitive deaminoNADH: decylubiquinone oxidoreductase activities normalized to complex I content (100% = 0,52 μmol·min^{-1}·mg^{-1}), (B) inhibitor sensitive deaminoNADH oxidase activity involving electron transfer from complex I to native Q9 in the membrane. Color scheme see Fig. 1. (For interpretation of the references to color in this figure legend, the reader is referred to the web version of this article.)

conserved charged and polar residues (Fig. 1). Mutation of R97 and Q100 to alanine caused only a moderate decrease of Q reductase activity (see Methods), while mutant S94A showed wild type activity (Fig. 2). In contrast, a drastic drop in activity was found for D101A (Fig. 2). An interesting corollary emerged from the sequence analysis of this section; D101 is not strictly conserved in bacterial enzymes, and is typically replaced by an alanine residue (Figs. 1C and S3). Conversely, five positions downstream a glutamate residue is conserved in bacterial enzymes (see also Figs. 1C and S3), leaving a gap at the position in eukaryotic enzymes. This remarkable positional swapping, confirmed by co-evolution analysis using GREMLIN [50], suggests possible mechanistic enhancements from bacterial to mitochondrial enzymes that are concentrated in a critical region of the enzyme.

The exchange of the neighboring highly conserved R102 for alanine roughly halved the activity while mutant R102E showed a much smaller residual activity (Fig. 2). To understand the effect of the R102A mutation on substrate binding, we performed Michaelis-Menten kinetic experiments and observed that decyl-ubiquinone (DBQ) showed a small decrease in K_M (Fig. S4, Table S2). In the following short hydrophobic stretch (Fig. 1), I105A showed a minor decrease of activity but a roughly 50% drop in DBQ reductase activity was observed for mutant I106A. However, the K_M value for DBQ remained unchanged and similar to the wild type control. Interestingly, this mutant showed a much more drastic decrease in NADH oxidase activity of mitochondrial membranes strongly suggesting an impaired ubiquinone-9 (Q9) reductase activity. Introducing a phenylalanine at this position also caused a drastic loss of activity comparable to the exchange of the following F107 for alanine or proline (Fig. 2).

3.2. Mutations of residues of the highly conserved RXSPRQ motif of the PSST loop

Next, we studied the highly conserved RXSPRQ motif of the PSST loop, in which the residue R108 at the beginning can be singled out for several reasons. Its side chain points towards the center of the ca. 30 Å long Q access pathway and the corresponding residue in bovine complex I was suggested to critically interact with the isoprenoid side chain [16]. Moreover, the residue was recently shown to carry a rare hydroxyl modification in complex I from mammals [24,25]. The same modification of an arginine residue was also found in the active site loop of CO dehydrogenase that has a short stretch of sequence similarity with complex I subunit PSST in this region [51].

Based on mass spectrometry data for subunit PSST, we can exclude here that the hydroxylation of R108 occurs to a significant level in complex I from *Y. lipolytica* (Fig. S5, Table S5) and is therefore not essential for the bioenergetic core function of complex I. Mutation of

R108 to alanine showed only a moderate decrease in Vmax and K_M with different short chain Q analogues (Table S2). Likewise, Q9 dependent NADH oxidase activity was almost unchanged. However, a more drastic decrease of activity and a moderate increase in K_M value for DBQ was determined for mutant R108E, representing a net charge change of $-2e$. Interestingly, the residual activity of this mutant was significantly smaller for the electron transfer reaction to Q9 (12%) as compared with DBQ (35%). The substantial activity of the R108A and R108E mutants with DBQ permitted us to evaluate the capacity of the purified and reconstituted mutant enzymes to pump protons by measuring uncoupler and inhibitor sensitive ACMA quenching (Fig. S6). To account for the lower DBQ reductase activity of the mutants we adjusted electron transfer activity of the wild type control to approximately the same level using the inhibitor decyl-quinazolinamine (DQA). While for R108A we observed a minor decrease of proton translocation activity (Fig. S6A), the R108E mutant remarkably showed a drastic decline of proton pumping (Fig. S6B).

In contrast to the central position of R108, R112, the other highly conserved arginine residue of the RXSP**R**Q motif, is located somewhat outside the Q-tunnel (Figs. 1 and S1), Surprisingly, mutations R112A, R112E, R112H and R112K caused an even more drastic loss of activity (see below).

A series of mutants were also generated for residue A109 that is not strictly conserved. The exchange of A109 to glycine caused only a moderate decline of activity. Increasing the size and introducing a more hydrophilic character of the side chain decreased activity more drastically and a larger hydrophobic side chain blocked activity almost completely (Fig. 2). Kinetics with DBQ showed a decrease in Vmax and K_M values for mutants A109S and A109C (Table S2). Interestingly, a phenylalanine residue at this position caused a severe decrease of complex I content in mitochondrial membranes. Exchanges of S110 and Q113 drastically decreased activity (Fig. 2). In contrast, mutation of the highly conserved P111 and of the serine residue following the RXSPRQ motif caused only a very minor decrease of activity. Overall, extensive mutagenesis of conserved residues in the central loop of the PSST subunit revealed a number of amino acid residues that are central to Q reductase activity catalyzed by complex I.

3.3. Quinone binding and dynamics

In order to gain insights into the site-directed mutagenesis data at the molecular level, we performed fully atomistic classical MD simulations of WT and selected mutants. For a comprehensive analysis we included complex I from bacterial (*Thermus thermophilus*, *T.t.*, PDB id 4HEA), fungal (*Y. lipolytica*, *Y.l.*, PDB id 6GCS), and mammalian species (*Bos taurus*, *B.t.*, PDB id 5LC5). To avoid confusion and for direct comparison with the biochemical data, we here use uniformly the nomenclature and residue numbering for the enzyme complex from *Y. lipolytica*, i.e. also for corresponding residues in complex I from other species (see Table S3 for residue numbering in *T.t., B.t* and *Y.l.* enzymes). First, we analyzed the available structural data on complex I, which showed that the sidechain of the highly conserved R112 of the RXSP**R**Q motif (see above) shows large conformational variation together with the anionic E218 from ND1, with which it is found to form a salt-bridge in some of the structures of complex I (see Fig. S7). When MD simulations of WT enzyme were performed with a bound Q, the salt bridge rapidly stabilized with some fast opening-closing events observed (see panels A, C and E in Fig. 3). In contrast, when no such ion-pairing existed in the R112A mutant, the distance between anionic glutamate and alanine sidechain increased sharply to up to 15 Å (Fig. 4), complemented by the separation of backbone Cα of the two residues by more than 10 Å in a number of cases (Fig. S9). Remarkably, the ion-pair and the backbone dynamics of charged residues was found to be correlated with the movement of Q in the cavity (see Supplementary Video S1); as long as the Arg-Glu ion-pair stayed intact, the Q molecule remained in the tunnel (magenta and blue traces in Fig. 3). In contrast, the diffusion of Q towards the tunnel entrance was associated by a simultaneous dissociation of the ion-pair in *T.t.* and *B.t.* WT simulations (green traces in Fig. 3, panels A/B and E/F, see also Video S1). In the case of WT *Y.l.* simulations, the ion-pair remained closed most of the time (Fig. 3, panel C), and as a result Q did not escape towards the tunnel entrance. Instead, it explored alternative cavities in the protein ca. 30 Å away from N2 that formed transiently during the molecular dynamics (Fig. S10). In case of the R112A mutant no ion pair existed and the Q rapidly moved away from the binding site near N2 in the *Y.l.* and *B.t.* simulations. The behavior for *T.t.* simulations was somewhat different with two replicas showing slower relaxation of Q away from N2 (Fig. 4). Overall, we envisage an important role of the charged residues R112 in PSST and E218 in ND1 in coupling protein conformational dynamics to Q diffusion, which is likely to be central to redox-coupled proton pumping in complex I. In order to further test these coupled dynamics between the ion-pair and Q movement, we performed additional MD simulations of *B.t.* complex I by forcing the ion-pair dissociation by means of harmonic restraints (see Methods). These simulations showed departure of Q from the N2 binding site ca. 200 ns after the ion-pair dissociated, therefore, further substantiating our conclusions from unbiased equilibrium simulations (Fig. S11).

Notably, we also found that the intact Arg-Glu ion-pair made minimal charged interactions with the ND3 subunit in most of the simulation replicas, and only upon dissociation the positively charged arginine R112 formed additional ion-pairs with the conserved charged residue E39 in the loop between TMH1 and TMH2 of ND3 in *T.t.* and *B.t.* complex I (see Fig. S12). Similarly, anionic glutamate E218 participated in salt-bridge formation with different lysine residues in ND3 and ND1 (Fig. S12).

3.4. Quinone gating coupled to loop dynamics

In contrast to the distal position of R112, R108 occupies a central location in the PSST loop and sits right in the middle of the Q-tunnel (Figs. 1 and S1). We note that this arginine is unresolved in the crystal structure of *T.t.* enzyme and was therefore modeled in this work as part of the missing loop (see Computational methods). In WT simulations of all enzymes, we observed that the arginine R108 predominantly interacted with the conserved acidic residues that belong to the loop between TMH5 and TMH6 of ND1, (Fig. S13, panels A, C and E). To understand what type of structural rearrangements could occur upon mutating the central arginine, we performed MD simulations of the R108E mutant. The dissociation of the distal R112 (PSST)-E218 (ND1) ion pair as well as separation of the backbone Cα atoms were observed in a number of cases concomitant with the loosening of Q binding (see Figs. 4 and S9). However, in spite of that the Q molecules did not diffuse out entirely to the site near the Q-tunnel opening, instead were retained in the tunnel (Supplementary Video S2). Analysis of simulation trajectories revealed this occurred mainly due to the blockage created by extra ion-pairing between the glutamate residue in the mutant and conserved positively charged residues (see panels B, D and F in Fig. S13). We found that the anionic glutamate in the mutant strongly perturbed the tunnel structure and Q movement by forming salt bridges with a number of conserved residues. In the case of *T.t.* enzyme simulations, protonated H95 in the 49 kDa subunit interacted with glutamate for ca. 59% of simulation time (Fig. S13). In the *Y.l.* enzyme the glutamate interacted predominantly with R112 in the PSST loop, whereas positively charged residues R27 (ND1), R36 (ND1) and R102 (PSST) in *B.t.* enzyme simultaneously formed charged-charged interactions with the glutamate for about 69%, 42% and 62% of simulation time, respectively (Fig. S13). These data strongly corroborate the notion that a coordinated movement of charged residues is necessary for optimal Q diffusion in the tunnel.

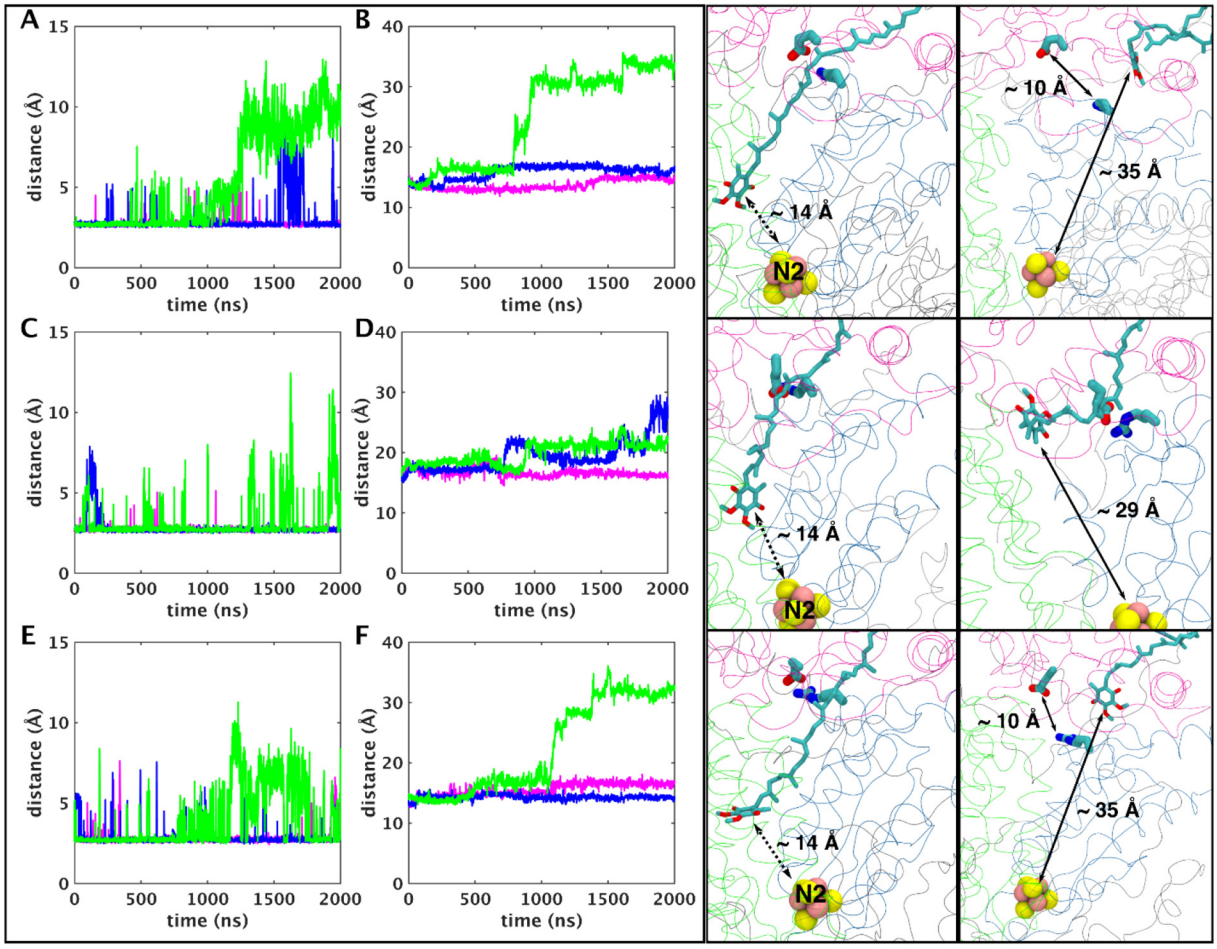

Fig. 3. Coupled dynamics of protein residues in the presence of Q.
Minimum distance between the sidechain polar atoms of R112 (PSST) and E218 (ND1) in (A) *T.t.*, (C) *Y.l.* and (E) *B.t.* WT systems with Q. Distance between the center of mass of FeS cluster N2 and the Q head group ring in (B) *T.t.*, (D) *Y.l.* and (F) *B.t.* WT systems with Q. Coupled dynamics of the ion pair and Q is shown on the right as simulation snapshots. Q at the bottom of the cavity is associated with the tight ion-pairing, but when dissociated, Q is released towards the entrance of the cavity, ca. 35 Å from the N2 center, complemented with ion-pair dissociation. In the case of *Y.l.* simulations, the ion-pair remains predominantly closed and Q explores additional cavities away from the N2 cluster. See also Fig. S8 for an alternative view. (For interpretation of the references to color in this figure, the reader is referred to the web version of this article.)

4. Discussion

The ubiquinone reduction site of respiratory complex I has a unique position ca. 30 Å from the surface of the membrane bilayer, not observed in any other respiratory enzyme. In this work, we have studied a conserved loop of subunit PSST that lines the access pathway for ubiquinone and forms an integral part of the functionally important interface region of membrane and peripheral arms.

With only one exception (A109F) all site-directed mutants generated in this study showed essentially unchanged NADH:HAR activity and unchanged abundance and migration behavior on BN gels indicating that overall structural stability or assembly of mutant complex I was not affected. Mutations at the N-terminal end of the PSST loop had only minor impact on Q reductase activity. The drastic effects caused by exchanges of acidic residues in the following sequence stretch presented here (D101) and in a previous study (D99) [26] can be explained by structural perturbations caused by disruption of salt bridges with residues in the loop following TMH1 of ND1. Indeed, our simulation data on *Y.l.* and *B.t.* complex I revealed charged interactions of D101 with conserved R27 and R36 from subunit ND1 (Fig. S14). Interestingly, these ion pairs remained stable for ca. 90% of simulation time (*B.t.* wild-type WT simulations) and were found to be partly perturbed by the movement of the Q in its access pathway (Fig. S14).

In the subsequent short hydrophobic segment I106 and F107 are of central importance for guiding the ubiquinone towards its reduction site near cluster N2. This is in agreement with structural data showing that the side chains of I106 and F107 are oriented towards the cavity (Fig. 1). In contrast, I105 points away from the Q tunnel and mutant I105A showed only a very minor decrease of activity. DBQ has a much shorter and linear side chain as compared with the isoprenoid side chain of the native Q9 in mitochondrial membranes of *Y. lipolytica*. The more drastic decrease in Q9 dependent activity for I106A suggests an important interaction of this hydrophobic residue with the isoprenoid tail that is less relevant for DBQ in agreement with an unchanged K_M value for this substrate. Introducing a phenylalanine at this position caused loss of activity with both substrates presumably by sterically blocking the access pathway. A109 is also close to the ubiquinone access pathway but assumes a position oriented more towards the TMH5/6 loop of ND1 and the β1-β2 loop of the 49-kDa subunit that forms part of the ubiquinone reduction site and was discussed to undergo functionally important conformational changes in the catalytic cycle [8]. Exchanges at this position might therefore on one hand impact ubiquinone access or on the other hand disturb structural rearrangements within the ubiquinone reduction site or both. The kinetics of A109S and A109C showed a decrease of Vmax and K_M for DBQ resembling an uncompetitive type of inhibition but providing no indication for a

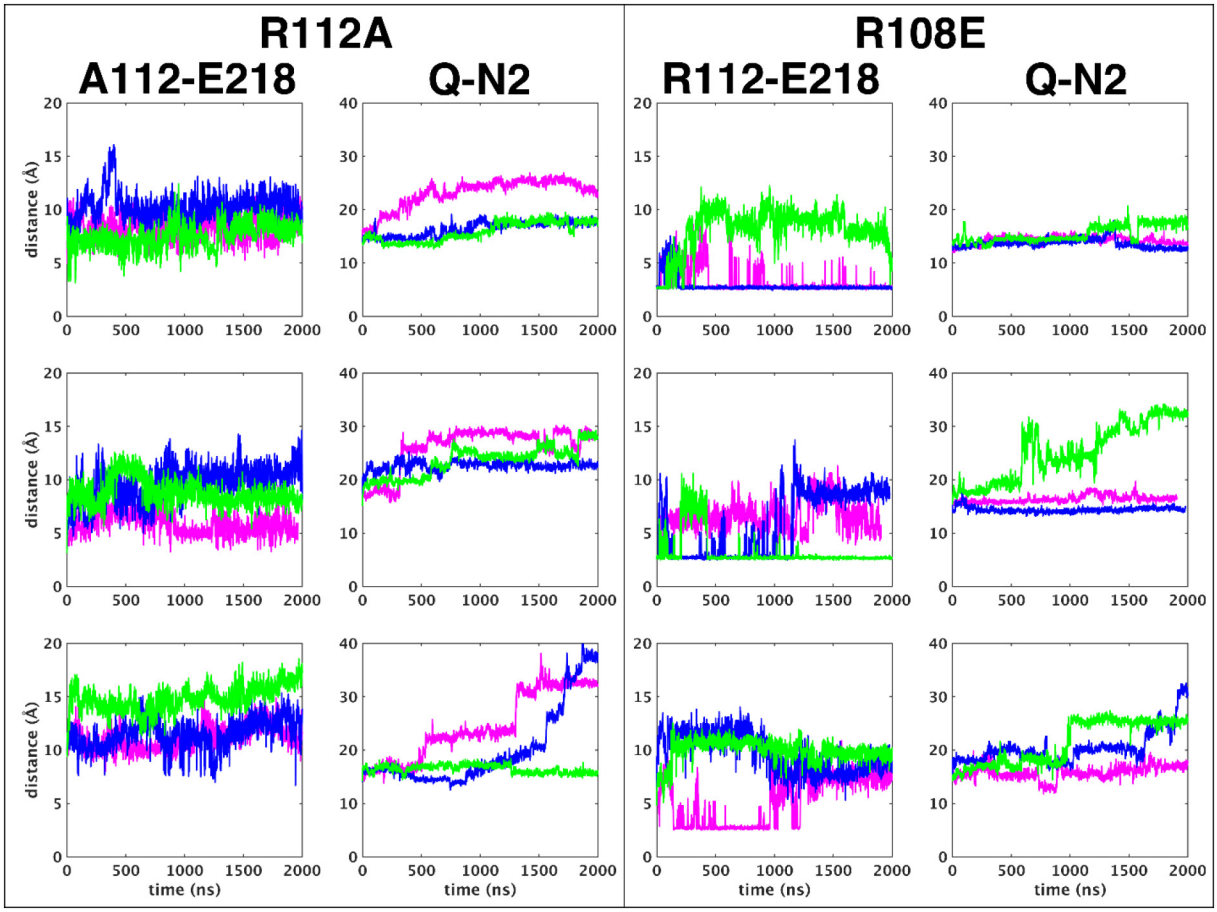

Fig. 4. Movement of Q in its access path in R112A and R108E mutant simulations.
Coupling between the dynamics of the R/A – E pair and Q movement are shown for R112A (left) and R108E (right) mutants. Minimum distance between the Cβ-atom of A112 (PSST, R112A mutant) or R112 (PSST, R108E mutant) and polar atoms of E218 (ND1) are shown in the plots and the corresponding Q-N2 distance, which is measured between the center of mass of iron-sulphur cluster N2 and the Q head group. The data is shown for *T.t.* (top panel), *Y.l.* (middle panel) and *B.t.* (lower panel) MD simulations and each simulation replica is shown in different colors (magenta, blue and green). (For interpretation of the references to color in this figure legend, the reader is referred to the web version of this article.)

decreased affinity of the substrate.

In mammalian complex I, the arginine residue corresponding to R108 in PSST of *Y. lipolytica* complex I was shown to be hydroxylated [24,25]. By mass spectrometry we showed here that this not a common post translational modification in *Y. lipolytica* complex I as reported before for complex Is from *Escherichia coli* and *Pichia pastoris* [24]. The functional significance of the arginine hydroxylation in mammals remains elusive. Nevertheless, it is clear that such a modification is not critical for the redox-coupled proton pumping in complex I and may be more important for the modulation of enzyme function in mammalian mitochondria.

In a study investigating kinetic properties of bovine complex I, Fedor et al. [16] had suggested that side chains of arginine residues corresponding to R102 and R108 in PSST of *Y. lipolytica* are engaged in networks with charged residues in subunit ND1 and are competent to form π stacking interactions with the long isoprenoid chain of Q10 (units 4 to 7). Given the central location of R108 in the Q-tunnel facing loop of the PSST subunit, its sidechain is likely to interact with the Q molecule. However, in contrast, the sidechain of R102 points away from the Q cavity in the majority of complex I structures [10,12–15]. Interestingly, exchanges of both arginine residues for alanine did not abolish the catalysis entirely but caused a decline of ubiquinone reductase activity, which was more pronounced for R102. The data from our microseconds *B.t.* simulations showed that the side chain of R102 formed ion-pairs with highly conserved acidic residues E26 and D53 of the ND1 subunit, which is also in agreement with the study by Fedor et al. [16]. Based on this, we envisage that the R102A mutant is likely to disturb the charged networks (and even stronger in the R102E mutant) in the Q-binding cavity thereby leading to lower Q reductase activity. The kinetic data for R102A and R108A mutants showed the same general behavior as observed for the A109 mutants thus providing no evidence for a decreased affinity for short chain Q analogues. The substantial activity of the R108A mutant with native Q9 demonstrated that the proposed π stacking interaction of this residue with the isoprenoid side chain [16] is not essential for ubiquinone reductase activity. Moreover, nearly unchanged behavior of mutant R108A in ACMA quench experiments showed that an arginine residue at this position is not critical for proton pumping. On the other hand, the drastic effects on ubiquinone reductase activity and proton pumping observed with the R108E mutant clearly demonstrated that inversion of the charge was not tolerated. Interestingly, R108 interacts with acidic residues in the loop connecting TMH 5 and 6 of subunit ND1. This loop represents the end point of the remarkable hydrophilic axis that extends from ND1 to the distal end of the membrane arm and is thought to be of central importance for triggering the proton pump elements of complex I [7,8]. While prohibiting ion pairing in the R108A mutant had surprisingly mild consequences the stronger effects of the R108E exchange might be explained by the larger charge imbalance introduced in the site. Moreover, simulations of R108E clearly showed that the charge inversion caused artificial charged-charged pairing between the glutamate and positively charged residues in the region that ultimately stalled Q movement in the tunnel (Video S2) and might also affect the

coupled electron/proton transfer reactions at the Q reduction site near N2 [52].

It is interesting to note that the decrease in activity of the R108E mutant was more pronounced for the electron transfer reaction to Q9 as compared with the short tailed DBQ. The reason for this could be that in the R108E mutant, the controlled movement of long tailed Q9 [16] through the entire tunnel length might be compromised by additional ion pairing by glutamate, whereas the shorter and more hydrophilic DBQ might even access the Q reduction site near FeS cluster N2 via an alternative pathway [53].

The strongest decline of activity for mutants in the C-terminal RXSP**R**Q motif was observed for R112. Even though the highly conserved R112 does not directly interact with the bound Q, mutation of this residue displayed a drastic effect on the Q reductase activity of complex I. Our simulation data revealed that R112 formed charged interactions with E218 of the ND1 subunit that stabilized Q in the tunnel with its head group near the N2 cluster. However, upon spontaneous dissociation or in the absence of the ion pair in the R/A mutant the head group of Q diffused towards the Q tunnel entrance thus supporting the notion of tight coupling between conformational dynamics of charged residues and Q movement (Video S1). The functional significance of E218 in ND1 is highlighted by the fact that mutation of the corresponding residue in human complex I (E214K) causes the mitochondrial encephalomyopathy, lactic acidosis and stroke-like episodes (MELAS) syndrome [54]. Since the ND1 gene is encoded by mitochondrial DNA, site-directed mutation of E218 is not possible in *Y. lipolytica*. Interestingly, exchanges of the residue in bacterial species, which would abolish or weaken the ion pairing with R112, had a major impact on assembly and activity of complex I [55,56].

We note that the R112 (PSST)-E218 (ND1) ion pair is located near the TMH1–2 loop of subunit ND3 that was recently shown to be of critical importance for redox-linked proton translocation [22] and is known to undergo conformational changes during the A/D transition of complex I [57]. It seems remarkable that R112 of PSST and E218 of ND1 formed transient interactions with conserved charged residues K34 and E39 in the ND3 loop in some of the simulations (Fig. S12) suggesting a tight structural rearrangement between the functionally critical PSST, ND1 and ND3 subunits, which may be important in the proton pumping mechanism of the enzyme in agreement with earlier mechanistic proposals [8]. Interestingly, mutation of the residue corresponding to E39 in *E.coli* complex I was shown to decrease dNADH:Q reductase activity to 30% [58].

Overall, the data from biochemical experiments and microsecond simulations of mitochondrial and bacterial enzymes provide first molecular insights in which a highly conserved Q-tunnel facing loop of the PSST subunit plays a crucial role in dynamics and diffusion of the bound Q.

Supplementary data to this article can be found online at https://doi.org/10.1016/j.bbabio.2019.06.006.

Transparency document

The Transparency document associated with this article can be found, in online version.

Acknowledgements

This work was supported by the Deutsche Forschungsgemeinschaft, grant ZI 552/4-1 to V.Z. and SFB815/Z1 to I.W., by the Excellence Initiative of the German Federal and State Governments (EXC 115 to V.Z.), by the research funding from the Academy of Finland (294652), the Sigrid Juséliuksen Säätiö and the University of Helsinki (to V.S.) and by the funds from CHEMS doctoral school of the University of Helsinki (to O.H.). The Center for Scientific Computing (CSC – IT Center for Science), Finland is acknowledged for generous computational resources, including the *Grand Challenge* resources. We acknowledge PRACE for awarding us access to MareNostrum at Barcelona Supercomputing Center (BSC), Spain.

References

[1] C. Wirth, U. Brandt, C. Hunte, V. Zickermann, Structure and function of mitochondrial complex I, Biochim. Biophys. Acta 1857 (2016) 902–914.
[2] J. Hirst, Mitochondrial complex I, Annu. Rev. Biochem. 82 (2013) 551–575.
[3] M. Wikstrom, V. Sharma, V.R. Kaila, J.P. Hosler, G. Hummer, New perspectives on proton pumping in cellular respiration, Chem. Rev. 115 (2015) 2196–2221.
[4] R.J. Rodenburg, Mitochondrial complex I-linked disease, Biochim. Biophys. Acta 1857 (2016) 938–945.
[5] E.T. Chouchani, C. Methner, S.M. Nadtochiy, A. Logan, V.R. Pell, S. Ding, A.M. James, H.M. Cocheme, J. Reinhold, K.S. Lilley, L. Partridge, I.M. Fearnley, A.J. Robinson, R.C. Hartley, R.A. Smith, T. Krieg, P.S. Brookes, M.P. Murphy, Cardioprotection by S-nitrosation of a cysteine switch on mitochondrial complex I, Nat. Med. 19 (2013) 753–759.
[6] A.B. Kotlyar, A.D. Vinogradov, Slow active/inactive transition of the mitochondrial NADH-ubiquinone reductase, Biochim. Biophys. Acta 1019 (1990) 151–158.
[7] R. Baradaran, J.M. Berrisford, G.S. Minhas, L.A. Sazanov, Crystal structure of the entire respiratory complex I, Nature 494 (2013) 443–448.
[8] V. Zickermann, C. Wirth, H. Nasiri, K. Siegmund, H. Schwalbe, C. Hunte, U. Brandt, Mechanistic insight from the crystal structure of mitochondrial complex I, Science 347 (2015) 44–49.
[9] J. Zhu, K.R. Vinothkumar, J. Hirst, Structure of mammalian respiratory complex I, Nature 536 (2016) 354–358.
[10] K. Fiedorczuk, J.A. Letts, G. Degliesposti, K. Kaszuba, M. Skehel, L.A. Sazanov, Atomic structure of the entire mammalian mitochondrial complex I, Nature 538 (2016) 406–410.
[11] J. Gu, M. Wu, R. Guo, K. Yan, J. Lei, N. Gao, M. Yang, The architecture of the mammalian respirasome, Nature 537 (2016) 639–643.
[12] R. Guo, S. Zong, M. Wu, J. Gu, M. Yang, Architecture of human mitochondrial respiratory megacomplex I2III2IV2, Cell 170 (2017) 1247–1257.
[13] J.N. Blaza, K.R. Vinothkumar, J. Hirst, Structure of the deactive state of mammalian respiratory complex I, Structure 26 (2018) 312–319.
[14] A.A. Agip, J.N. Blaza, H.R. Bridges, C. Viscomi, S. Rawson, S.P. Muench, J. Hirst, Cryo-EM structures of complex I from mouse heart mitochondria in two biochemically defined states, Nat. Struct. Mol. Biol. 25 (2018) 548–556.
[15] K. Parey, U. Brandt, H. Xie, D.J. Mills, K. Siegmund, J. Vonck, W. Kuhlbrandt, V. Zickermann, Cryo-EM structure of respiratory complex I at work, Elife 7 (2018).
[16] J.G. Fedor, A.J.Y. Jones, A. Di Luca, V.R.I. Kaila, J. Hirst, Correlating kinetic and structural data on ubiquinone binding and reduction by respiratory complex I, Proc. Natl. Acad. Sci. U. S. A. 114 (2017) 12737–12742.
[17] H. Angerer, H.R. Nasiri, V. Niedergesass, S. Kerscher, H. Schwalbe, U. Brandt, Tracing the tail of ubiquinone in mitochondrial complex I, Biochim. Biophys. Acta 1817 (2012) 1776–1784.
[18] V.R.I. Kaila, Long-range proton-coupled electron transfer in biological energy conversion: towards mechanistic understanding of respiratory complex I, J. R. Soc. Interface 15 (2018).
[19] O. Haapanen, V. Sharma, A modeling and simulation perspective on the mechanism and function of respiratory complex I, Biochim. Biophys. Acta 1859 (2018) 510–523.
[20] J. Warnau, V. Sharma, A.P. Gamiz-Hernandez, A. DiLuca, O. Haapanen, I. Vattulainen, M. Wikstrom, G. Hummer, V.R.I. Kaila, Redox-coupled quinone dynamics in the respiratory complex I, Proc. Natl. Acad. Sci. U. S. A. 115 (2018) E8413–E8420.
[21] U. Brandt, A two-state stabilization-change mechanism for proton-pumping complex I, Biochim. Biophys. Acta 1807 (2011) 1364–1369.
[22] A. Cabrera-Orefice, E.G. Yoga, C. Wirth, K. Siegmund, K. Zwicker, S. Guerrero-Castillo, V. Zickermann, C. Hunte, U. Brandt, Locking loop movement in the ubiquinone pocket of complex I disengages the proton pumps, Nat. Commun. 9 (2018) 4500.
[23] M.A. Tocilescu, V. Zickermann, K. Zwicker, U. Brandt, Quinone binding and reduction by respiratory complex I, Biochim. Biophys. Acta 1797 (2010) 1883–1890.
[24] J. Carroll, S. Ding, I.M. Fearnley, J.E. Walker, Post-translational modifications near the quinone binding site of mammalian complex I, J. Biol. Chem. 288 (2013) 24799–24808.
[25] V.F. Rhein, J. Carroll, S. Ding, I.M. Fearnley, J.E. Walker, NDUFAF5 hydroxylates NDUFS7 at an early stage in the assembly of human complex I, J. Biol. Chem. 291 (2016) 14851–14860.
[26] A. Garofano, K. Zwicker, S. Kerscher, P. Okun, U. Brandt, Two aspartic acid residues in the PSST-homologous NUKM subunit of complex I from Yarrowia lipolytica are essential for catalytic activity, J. Biol. Chem. 278 (2003) 42435–42440.
[27] D.C. Chen, J.M. Beckerich, C. Gaillardin, One-step transformation of the dimorphic yeast Yarrowia lipolytica, Appl. Microbiol. Biotechnol. 48 (1997) 232–235.
[28] N. Kashani-Poor, S. Kerscher, V. Zickermann, U. Brandt, Efficient large scale purification of his-tagged proton translocating NADH:ubiquinone oxidoreductase (complex I) from the strictly aerobic yeast Yarrowia lipolytica, Biochim. Biophys. Acta 1504 (2001) 363–370.
[29] Kinetics of the mitochondrial three-subunit NADH dehydrogenase interaction with hexammineruthenium(III). Gavrikova EV, Grivennikova VG, Sled VD, Ohnishi T, Vinogradov AD. Biochim. Biophys. Acta. 1995 Jun 1;1230(1-2):23-30.
[30] S. Drose, A. Galkin, U. Brandt, Proton pumping by complex I (NADH:ubiquinone oxidoreductase) from Yarrowia lipolytica reconstituted into proteoliposomes,

Biochim. Biophys. Acta 1710 (2005) 87–95.
[31] I. Wittig, R. Carrozzo, F.M. Santorelli, H. Schagger, Supercomplexes and subcomplexes of mitochondrial oxidative phosphorylation, Biochim. Biophys. Acta 1757 (2006) 1066–1072.
[32] I. Wittig, M. Karas, H. Schagger, High resolution clear native electrophoresis for in-gel functional assays and fluorescence studies of membrane protein complexes, Mol. Cell. Proteomics 6 (2007) 1215–1225.
[33] J. Rappsilber, M. Mann, Y. Ishihama, Protocol for micro-purification, enrichment, pre-fractionation and storage of peptides for proteomics using StageTips, Nat. Protoc. 2 (2007) 1896–1906.
[34] A. Sali, T.L. Blundell, Comparative protein modelling by satisfaction of spatial restraints, J. Mol. Biol. 234 (1993) 779–815.
[35] S. Jo, T. Kim, V.G. Iyer, W. Im, CHARMM-GUI: a web-based graphical user interface for CHARMM, J. Comput. Chem. 29 (2008) 1859–1865.
[36] B.R. Brooks, C.L. Brooks III, A.D. Mackerell Jr., L. Nilsson, R.J. Petrella, B. Roux, Y. Won, G. Archontis, C. Bartels, S. Boresch, A. Caflisch, L. Caves, Q. Cui, A.R. Dinner, M. Feig, S. Fischer, J. Gao, M. Hodoscek, W. Im, K. Kuczera, T. Lazaridis, J. Ma, V. Ovchinnikov, E. Paci, R.W. Pastor, C.B. Post, J.Z. Pu, M. Schaefer, B. Tidor, R.M. Venable, H.L. Woodcock, X. Wu, W. Yang, D.M. York, M. Karplus, CHARMM: the biomolecular simulation program, J. Comput. Chem. 30 (2009) 1545–1614.
[37] J. Lee, X. Cheng, J.M. Swails, M.S. Yeom, P.K. Eastman, J.A. Lemkul, S. Wei, J. Buckner, J.C. Jeong, Y. Qi, S. Jo, V.S. Pande, D.A. Case, C.L. Brooks III, A.D. Mackerell Jr., J.B. Klauda, W. Im, CHARMM-GUI input generator for NAMD, GROMACS, AMBER, OpenMM, and CHARMM/OpenMM simulations using the CHARMM36 additive force field, J. Chem. Theory Comput. 12 (2016) 405–413.
[38] M.A. Lomize, I.D. Pogozheva, H. Joo, H.I. Mosberg, A.L. Lomize, OPM database and PPM web server: resources for positioning of proteins in membranes, Nucleic Acids Res. 40 (2012) D370–D376.
[39] O. Haapanen, V. Sharma, Role of water and protein dynamics in proton pumping by respiratory complex I, Sci. Rep. 7 (2017) 7747.
[40] S. Nosé, A unified formulation of the constant temperature molecular dynamics methods, J. Chem. Phys. 81 (1984) 511–519.
[41] W.G. Hoover, Canonical dynamics: equilibrium phase-space distributions, Phys. Rev. A 31 (1985) 1695–1697.
[42] M. Parrinello, A. Rahman, Polymorphic transitions in single crystals: a new molecular dynamics method, J. Appl. Phys. 52 (1981) 7182–7190.
[43] M. Parrinello, A. Rahman, Crystal structure and pair potentials: a molecular-dynamics study, Phys. Rev. Lett. 45 (1980) 1196.
[44] M.J. Abraham, T. Murtola, R. Schulz, S. Páll, J.C. Smith, B. Hess, E. Lindahl, GROMACS: high performance molecular simulations through multi-level parallelism from laptops to supercomputers, SoftwareX 1 (2015) 19–25.
[45] A.D. MacKerell, M. Feig, C.L. Brooks, Extending the treatment of backbone energetics in protein force fields: limitations of gas-phase quantum mechanics in reproducing protein conformational distributions in molecular dynamics simulations, J. Comput. Chem. 25 (2004) 1400–1415.
[46] A.D. MacKerell Jr., D. Bashford, M.L.D.R. Bellott, R.L. Dunbrack Jr., J.D. Evanseck, M.J. Field, S. Fischer, J. Gao, H. Guo, S. Ha, All-atom empirical potential for molecular modeling and dynamics studies of proteins, J. Phys. Chem. B 102 (1998) 3586–3616.
[47] J.B. Klauda, R.M. Venable, J.A. Freites, J.W. O´Connor, D.J. Tobias, C. Mondragon-Ramirez, I. Vorobyov, A.D. MacKerell Jr., R.W. Pastor, Update of the CHARMM all-atom additive force field for lipids: validation on six lipid types, J. Phys. Chem. B 114 (2010) 7830–7843.
[48] V.V. Galassi, G.M. Arantes, Partition, orientation and mobility of ubiquinones in a lipid bilayer, Biochim. Biophys. Acta 1847 (2015) 1560–1573.
[49] C.H. Chang, K. Kim, Density functional theory calculation of bonding and charge parameters for molecular dynamics studies on [FeFe] hydrogenases, J. Chem. Theory Comput. 5 (2009) 1137–1145.
[50] S. Ovchinnikov, H. Kamisetty, D. Baker, Robust and accurate prediction of residue-residue interactions across protein interfaces using evolutionary information, Elife 3 (2014) e02030.
[51] P. Hanzelmann, H. Dobbek, L. Gremer, R. Huber, O. Meyer, The effect of intracellular molybdenum in Hydrogenophaga pseudoflava on the crystallographic structure of the seleno-molybdo-iron-sulfur flavoenzyme carbon monoxide dehydrogenase, J. Mol. Biol. 301 (2000) 1221–1235.
[52] V. Sharma, G. Belevich, A.P. Gamiz-Hernandez, T. Rog, I. Vattulainen, M.L. Verkhovskaya, M. Wikstrom, G. Hummer, V.R. Kaila, Redox-induced activation of the proton pump in the respiratory complex I, Proc. Natl. Acad. Sci. U. S. A. 112 (2015) 11571–11576.
[53] O. Haapanen, A. Djurabekova, V. Sharma, Role of second quinone binding site in proton pumping by respiratory complex I, Front. Chem. 7 (2019) 221.
[54] D.M. Kirby, R. McFarland, A. Ohtake, C. Dunning, M.T. Ryan, C. Wilson, D. Ketteridge, D.M. Turnbull, D.R. Thorburn, R.W. Taylor, Mutations of the mitochondrial ND1 gene as a cause of MELAS, J. Med. Genet. 41 (2004) 784–789.
[55] M. Kervinen, R. Hinttala, H.M. Helander, S. Kurki, J. Uusimaa, M. Finel, K. Majamaa, I.E. Hassinen, The MELAS mutations 3946 and 3949 perturb the critical structure in a conserved loop of the ND1 subunit of mitochondrial complex I, Hum. Mol. Genet. 15 (2006) 2543–2552.
[56] P.K. Sinha, J. Torres-Bacete, E. Nakamaru-Ogiso, N. Castro-Guerrero, A. Matsuno-Yagi, T. Yagi, Critical roles of subunit NuoH (ND1) in the assembly of peripheral subunits with the membrane domain of *Escherichia coli* NDH-1, J. Biol. Chem. 284 (2009) 9814–9823.
[57] A. Galkin, B. Meyer, I. Wittig, M. Karas, H. Schagger, A. Vinogradov, U. Brandt, Identification of the mitochondrial ND3 subunit as a structural component involved in the active/deactive enzyme transition of respiratory complex I, J. Biol. Chem. 283 (2008) 20907–20913.
[58] M.C. Kao, B.S. Di, M. Perego, E. Nakamaru-Ogiso, A. Matsuno-Yagi, T. Yagi, Functional roles of four conserved charged residues in the membrane domain subunit NuoA of the proton-translocating NADH-quinone oxidoreductase from Escherichia coli, J. Biol. Chem. 279 (2004) 32360–32366.
[59] E. Chovancova, A. Pavelka, P. Benes, O. Strnad, J. Brezovsky, B. Kozlikova, A. Gora, V. Sustr, M. Klvana, P. Medek, L. Biedermannova, J. Sochor, J. Damborsky, CAVER 3.0: a tool for the analysis of transport pathways in dynamic protein structures, PLoS Comput. Biol. 8 (2012) e1002708.